12

Aerosol Radiative Forcing: AERONET-Based Estimates

O.E. García[1], J.P. Díaz[2], F.J. Expósito[2], A.M. Díaz[2],
O. Dubovik[3] and Y. Derimian[3]
[1]*Centro de Investigación Atmosférica de Izaña, Agencia Estatal de Meteorología (AEMET)*
[2]*Grupo de Observación de la Tierra y la Atmósfera, Universidad de La Laguna*
[3]*Laboratoire d'Optique Amosphérique, Université Lille1,*
[1,2]*Spain*
[3]*France*

1. Introduction

Solar radiation is the main source of energy for the Earth-atmosphere system, and directly or indirectly, is responsible for all phenomena affecting the meteorology and climatology of this system. The variation of any component of this system affects the radiative equilibrium, resulting in, for example, changes in the temperature of the system and/or in the configuration of the atmospheric circulation. In order to quantify these effects the concept of radiative forcing was introduced in the literature to show the magnitude of radiation variation due to changes in a specific atmospheric component, for instance, clouds, gases or atmospheric aerosols.

One of the main reasons for the changes in the energy balance of the Earth-atmosphere system is the variation in the concentration of greenhouse gases, GHGs, which contribute to an increase in the system temperature. On a global scale, the total annual anthropogenic emissions of GHGs have increased 70% between 1970 and 2004 with respect to the pre-industrial era. The associated radiative forcing of this increase is expected to be +2.3 Wm^{-2}, with an uncertainty of ±0.2 Wm^{-2} (IPCC, 2007).

On the other hand, another decisive factor is atmospheric aerosol, both from natural and anthropogenic origin. These atmospheric constituents, directly and indirectly, modify the energy balance of the Earth-atmosphere system: directly through the absorption and dispersion of solar radiation in the atmosphere and, indirectly, by acting as nuclei of cloud condensation, and modifying their own properties (albedo, reflectivity, lifetime, precipitation efficiency,...) (Charlson et al., 1987; Lohmann & Fiechter, 2005; Twomey, 1977). Finally, there are semi-direct effects associated with the absorption of solar radiation by aerosols. These produce an unequal warming of the atmosphere, favouring unstable conditions and also contributing to the modification of cloud characteristics (Ackerman et al., 2000; Koren et al., 2004).

Even though the impact of atmospheric aerosols on climate (and climatic change) is undeniable, the knowledge of their radiative forcing (direct, semi-direct and indirect effects)

is still not well understood (IPCC, 2007). The radiative effects of these atmospheric constituents depend largely on their size distributions and their chemical composition. Thus, on a global scale, the direct radiative forcing of sulphates is estimated to be -0.4±0.2 Wm^{-2}, of organic carbon -0.05±0.05 Wm^{-2}, for soot, +0.20±0.15 Wm^{-2}, while aerosol radiative forcing from natural origins such as biomass burning and mineral dust are +0.03±0.12 Wm^{-2} and -0.1±0.2 Wm^{-2} respectively (IPCC, 2007). Although the local effects can be far greater and reach hundreds of Wm^{-2}, mainly in those regions close to the emission sources (García et al., 2011a, 2011b; Haywood et al., 2003). These values clearly indicate significant uncertainties in the aerosol radiative forcing estimates and confirm the need to study their radiative properties and to quantify their effects on radiative balance.

According to the recent report of Intergovernmental Panel on Climate Change (2007), the direct radiative forcing of the individual aerosol species is less certain than the total direct radiative forcing by all aerosols. Likewise, recent studies show that most climate models underestimate the negative forcing by anthropogenic aerosols (Hansen et al., 2011). In this context, the long-term monitoring of different aerosol types is crucial to improve our knowledge of the radiative forcing and climate parameters. Nowadays, one of the most useful tools supporting this aim is the AErosol RObotic NETwork (AERONET, http://aeronet.gsfc.nasa.gov), which provides enough information globally to establish a ground-based aerosol climatology. An extended set of physical and optical aerosol properties, averaged in the atmospheric column (Dubovik et al., 2002a, 2006) and given at more than 180 worldwide locations, have enabled verification of global aerosol models and satellite retrievals.

Thus, this chapter describes an approach to evaluate the direct radiative effect of atmospheric aerosols from AERONET observations. The radiative net effect of key aerosol types is discussed with a homogeneous methodology, which allows a direct intercomparison and establishment of a climatology, for example, to feed into climate models or for technical proposals. To that end, the AERONET network (database, radiative transfer model and its validation) is presented in section 2, while section 3 shows a climatology of the direct radiative forcing of key aerosol types at the bottom and at the top of atmosphere. Finally, the main remarks are summarized in the section 4.

2. AErosol RObotic NETwork (AERONET)

2.1 AERONET Database

AERONET is one of the most useful global networks for monitoring atmospheric aerosols. It collects near real time observations of spectral and columnar integrated aerosol optical properties. These data are collected by automatic sun and sky scanning spectral radiometers manufactured by CIMEL Electronique and they are distributed to worldwide locations. The direct sun measurements are performed by the CIMEL radiometers on all or some of the following channels: 0.34, 0.38, 0.44, 0.50, 0.67, 0.87, 0.94, 1.02 and 1.64 μm (nominal wavelengths) with a field of view of 1.2 degrees. Then, the aerosol optical depth (AOD) is retrieved at all these wavelengths except at 0.94 μm, which is used to estimate total precipitable water content. In addition to the direct solar radiance measurements, these instruments measure the sky radiance in four spectral bands (0.44, 0.67, 0.87 and 1.02 μm) along both the solar principal plane and the solar almucantar.

Solar aureole/sky radiance together with sun measurements are used to retrieve aerosol volume size distributions ($dV(r)/d\ln(r)$ from 0.05 to 15 μm), spectral complex refractive index ($m(\lambda)$-i$k(\lambda)$) and single scattering albedo ($\omega(\lambda)$) at low solar elevations (solar zenith angles, sza, between 50º and 80º), following a flexible inversion algorithm developed by Dubovik & King (2000) (Version 1.0 inversion products). This algorithm uses models of homogeneous spheres and randomly oriented spheroids (Dubovik et al., 2002a). Recently a new version of this inversion algorithm, Version 2.0, has been developed. The most significant improvement is the use of a spheroid mixture as a generalized aerosol model (representing spherical, non-spherical and mixed aerosols, with shape parameter between 0.3 and 3.0) (Dubovik et al., 2006), and replacing the spherical and spheroid models used separately up to now. In this vein, the Version 2.0 provides a parametrization of the degree of non-sphericity (sphericity parameter), as well as the same set of retrieved aerosol parameters given in the Version 1.0. The AERONET inversion scheme is clearly summarized in paper by Dubovik et al., (2011).

The appropriate characterization of the surface albedo is a critical issue to estimate aerosol radiative effect (Myhre et al., 2003) as well as an important error source in the retrieval of aerosol properties (Dubovik et al., 2000; Sinyuk et al., 2007). For that reason, one of the most important improvements in the Version 2.0 is the assumption of a dynamic spectral and spatial satellite and model estimation of the surface reflectivity (SR), including the bidirectional reflectance distribution function (BRDF), in the place of an assumed surface reflectivity (Dubovik et al., 2000). Thus, the BRDF Cox-Munk model over water was used, which takes the wind effect over water into account by using the wind speed data from NCEP/NCAR database (NOAA National Weather Service NOMADS NCEP server). For land surface covers, the Lie-Ross model was adopted, where the BRDF parameters are taken from the MODIS Ecotype generic BRDF models for vegetation, snow and ice (http://aeronet.gsfc.nasa.gov). Finally, another important addition in the AERONET inversion products Version 2.0 is that a set of radiative magnitudes are estimated at any AERONET station: spectral and broadband fluxes, besides aerosol radiative forcing and aerosol radiative forcing efficiency at the bottom of the atmosphere (BOA) and at the top of atmosphere (TOA), which allow to study the radiative effects under different aerosol regimes. The AERONET radiative transfer model used to estimate them is explained in detail in the subsection 2.2, while the validation of AERONET solar flux estimates is shown in the subsection 2.3.

The level of accuracy in the CIMEL measurements is a critical issue in the inversion process, since the retrieval algorithm is set to fit the data to the level of AERONET measurement uncertainty, i.e., the nominal error in AOD is assumed 0.015·cos (sza), while for sky radiance measurements the error is ±5%. These values are determined by calibration conditions. For the direct measurements, the calibration of field instruments is performed by a transfer of the calibration from reference CIMELs, which are calibrated by the Langley plot technique at Mauna Loa Observatory (Hawaii). Typically, the total uncertainty in spectral aerosol optical depth for the field instruments ranges from 0.01 to 0.02 under cloud-free conditions for air mass equal one (Eck et al., 1999), with the highest errors (0.02) associated with the ultraviolet wavelengths. For the sky radiance measurements, the calibration is performed by comparing to a reference integrating sphere with an accuracy of ±5% or better at the NASA

Goddard Calibration Facility (Holben et al., 1998). Regarding the long-term stability of the calibration coefficients, the optical interference filters are the main limiting factors. On average, a decrease from 0 to ~5% per year is expected, depending largely on material deposition on the optics.

The AERONET aerosol products are computed for three data quality levels: Level 1.0 (unscreened), Level 1.5 (cloud-screened), and Level 2.0 (cloud-screened and quality-assured) (http://aeronet.gsfc.nasa.gov). The AERONET data used in this study are taken from the highest quality version under clear-sky conditions, i.e., Version 2.0 at level 2.0.

2.2 AERONET radiative transfer approach

As part of the efforts to enhance the value of retrieval products, a new radiative transfer module has been integrated into operational AERONET inversion code. This module uses the detailed size distribution, complex refractive index and fraction of spherical particles retrieved by AERONET (Dubovik and King, 2000, Dubovik et al. 2006) and provides the fluxes and aerosol radiative forcing values as part of AERONET operational product. Similar to the AERONET retrieval, the AERONET computations of solar fluxes account for the absorption and multiple scattering effects using the Discrete Ordinates DISORT approach (Nakajima & Tanaka, 1988; Stamnes et al., 1988). The solar broadband fluxes are calculated by spectral integration from 0.2 to 4.0 μm, using more than 200 size sub-intervals. In each of these sub-intervals the extinction, single scattering albedo and phase function are calculated using the retrieved size distribution in the exact same manner as in the AERONET retrieval scheme. The values of $m(\lambda)$ and $k(\lambda)$ are linearly interpolated and extrapolated from the values $m(\lambda)$ and $k(\lambda)$ retrieved at the AERONET wavelengths. Likewise, the spectral dependence of surface reflectance is linearly interpolated and extrapolated from surface albedo values assumed in the retrieval of the sun/sky-radiometer measurements. Note that the AERONET solar fluxes are only evaluated for solar zenith angles between 50^o and 80^o, where the solar geometry conditions are the most appropriate for retrieving the aerosol properties (Dubovik et al., 2002b, 2000).

The integration of atmospheric aerosol scattering and absorption, gaseous absorption, molecular scattering and underlying surface reflection effects are conducted using developments employed in the GAME (Global Atmospheric ModEl) code (Dubuisson et al. 1996; Roger et al., 2006). In the GAME code, gaseous absorption (mainly H_2O, CO_2 and O_3), is calculated from the correlated k-distribution. The correlated k-distribution allows for the interactions between gaseous absorption and multiple scattering to be accounted for with manageable computational time. Coefficients of the correlated k-distribution were estimated from reference calculations using a line-by line code (Dubuisson et al., 2004). Regarding the gaseous content in the atmospheric column, the GAME model accounts for spectral gaseous absorption: ozone in the ultraviolet-visible spectral range (0.2-0.35 μm and 0.5-0.7 μm) and water vapour in the shortwave infrared spectrum (0.8-3 μm). The instantaneous water vapour content retrieved by AERONET (Smirnov et al. 2000) is employed, while the total ozone content is taken from monthly climatology values (1978-2004) based on the NASA Total Ozone Mapping Spectrometer (TOMS) measurements (http://jwocky.gsfc.nasa.gov/). The atmospheric gaseous profile, US standard 1976 atmosphere model, was scaled to match

with the gaseous concentrations in column. The GAME code has a fixed spectral resolution of 100 cm^{-1} from 2500 to 17700 cm^{-1} (4 to 0.6 μm) and 400 cm^{-1} from 17700 cm^{-1} to 50000 cm^{-1} (0.6 to 0.2 μm).

The AERONET calculation of broadband radiation is focused on accurate accounting for the spectral dependence of the aerosol optical properties and surface reflectivity used as inputs. Recent studies showed that both to neglect completely the spectral dependence and to consider only specific spectral range of aerosol properties are important error sources. These studies found uncertainties up to 30% for total aerosol radiative effect, combining the spectral influence and solar zenith angle variation (Myhre et al., 2003; Zhou et al., 2005). Also, it should be noted that in contrast with simplified approaches (accounting only for asymmetry of phase function) flux calculations employed in AERONET processing use the detailed phase function (12 moments).

As aforementioned, the radiative forcing is introduced in literature to account for changes in the solar radiation levels due to changes in the atmospheric constituents. Hence, the direct radiative forcing of atmospheric aerosols, denoted as ΔF, is defined as the difference in the energy levels between a situation where aerosols are present, F^A, and a situation where these atmospheric particles are absent, F^C. AERONET estimates these values at the BOA and the TOA. Thus, radiative forcing can be defined at these two levels as:

$$\Delta F_{BOA} = F_{BOA}{}^{\downarrow A} - F_{BOA}{}^{\downarrow C} \quad (1)$$

$$\Delta F_{TOA} = F_{TOA}{}^{\uparrow C} - F_{TOA}{}^{\uparrow A} \quad (2)$$

where the arrows indicate the direction of the solar global fluxes: ↓ ≡ downward flux and ↑ ≡ upward flux, which are computed as aforementioned. This sign criterion implies that negative values of ΔF at the BOA and at the TOA are associated with an aerosol cooling effect, while a warming effect is due to positive values of ΔF at the BOA and at the TOA. In climate applications it is also often used the net radiative forcing, which is defined at the BOA as:

$$\Delta F_{BOA\ net} = F_{BOA}{}^{A} - F_{BOA}{}^{C} \quad (3)$$

where $F_{BOA}{}^{C}$ and $F_{BOA}{}^{A}$ are the net (downwelling minus upwelling) fluxes in aerosol absent and aerosol present situations, respectively. Therefore, the net BOA forcing accounts for interaction with the surface and depends on the surface reflectance. At the TOA the values of the net forcing are identical to what can be found from the equation (2) because at the TOA the downwelling (extraterrestrial) flux is the same either for aerosol absent or aerosol present conditions.

The aerosol radiative forcing strongly depends on solar geometry, so the ΔF results presented in this work (section 3) have been limited to a narrow interval of solar zenith angles (60 ± 5^{o}), where the maximal number of AERONET retrievals are assembled. The whole AERONET scheme, including the inversion process and the simulation of solar fluxes, is summarized in the Fig. 1.

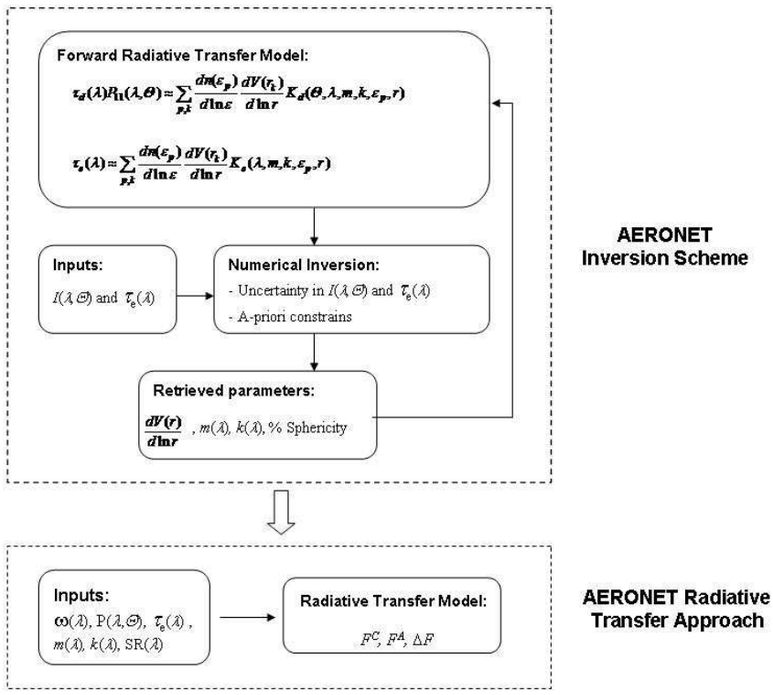

Fig. 1. AERONET scheme to compute solar broadband fluxes: AERONET inversion scheme (Dubovik et al., 2006) and AERONET Radiative Transfer approach.

2.3 Validation of AERONET solar flux estimates

High quality solar flux estimates, and hence aerosol radiative forcing values, are crucial to properly analyze annual cycles and possible trends. Furthermore, such high quality reference data are needed in order to document the quality and consistency of data obtained from space-based sensors or climate model simulations. Therefore, the intercomparison with observed solar measurements is mandatory. Thus, the AERONET broadband flux estimates have been validated in recent works by using ground-based solar measurements from global networks and during intensive field campaigns (Derimian et al., 2008; García et al., 2008). As a result, AERONET solar fluxes agree with solar observations within 10% or better.

García et al., (2008), using ground-based solar measurements under different aerosol environments, found that the straight forward comparison between the observed and modeled solar irradiance shows an excellent agreement (slope of 0.98±0.00 and bias of -5.32±1.00 Wm^{-2}), with a correlation of 99% (see Fig. 2). As a result, in global terms, a small overestimation of +9±12 Wm^{-2} is found on the observed solar radiation at surface, which means a relative error of +2.1±3.0%. For each aerosol type, these differences range from -2±8 to -3±7 Wm^{-2} under continental background, from +8±9 to +16±10 Wm^{-2} for stations with mineral dust conditions, +14±10 Wm^{-2} and +6±13 Wm^{-2} for urban-industrial and biomass burning aerosols respectively, lower than +13±10 Wm^{-2} under oceanic environments and +2±10 Wm^{-2} in the free troposphere conditions observed in the Mauna Loa Observatory. These errors are expected to be of the same magnitude at the TOA, since the same methodology is used at both levels (gaseous and aerosol distribution, radiative model, etc).

These differences could be attributed, partly, to the combination of instrumental errors such as cosine response, calibration, linearity, etc., in the pyranometer measurements. All of these error sources usually give uncertainties of less than 3%-5% of the instantaneous instrument signal (Dutton et al., 2001). Given the solar zenith angle range used to AERONET sky measurements (50º-80º), one of the most influencing factor is the non-ideal angular response of this type of instruments, which limits their accuracy to about 3%, or 20-30 Wm^{-2}, for instantaneous clear-sky measurements (Michalsky et al., 1999). This effect would result in measured flux that is biased low relative to true flux, resulting thus the overestimation observed in the AERONET solar broadband fluxes.

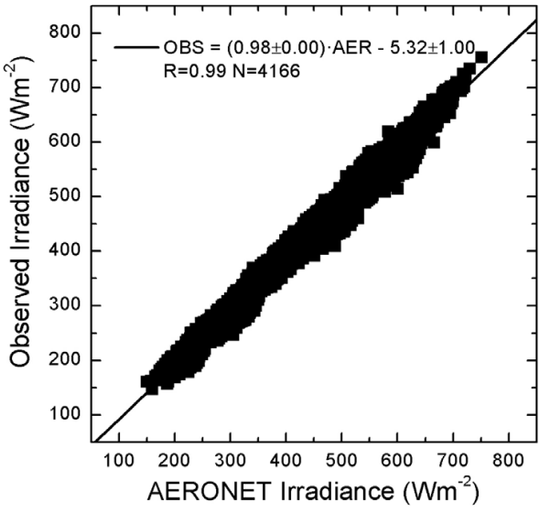

Fig. 2. Comparison between the solar irradiance (Wm^{-2}) observed by ground-based pyranometer and modelled with AERONET inputs at surface (García et al., 2008). The legend shows the least square fit parameters.

In addition to the instrumental uncertainties, the uncertainty in surface albedo and BRDF, assumed by AERONET, must also be considered as a potential error source in the modeled downwelling fluxes. This is especially true for the locations dominated by mineral dust, where the surface albedo is usually quite bright. In such conditions, the values managed in AERONET may be higher than real ones, providing an overestimation of the observed irradiance as was shown previously. This artefact will be more pronounced for high aerosol load due to the multiple scattering processes. Besides the uncertainties in the surface albedo for large solar zenith angles must be taken into account in the error interpretation.

Model assumptions as the homogeneous aerosol vertical structure considered in AERONET retrievals can be considered also as sources of uncertainties; however the effect of these errors is minor in most cases (Dubovik et al., 2000). The flux calculations are performed for multi-layered atmosphere with US standard atmosphere model for gaseous distributions and single fixed aerosol vertical distribution (exponential with aerosol height of 1 km). The deviations of these assumptions from reality are also potential source of errors, although, our tests did not show any significant sensitivity of flux estimates to these assumptions. Differences less than 1 Wm^{-2} due to different vertical profiles were observed on the downward solar flux at the bottom of the atmosphere (García et al., 2008). These differences are negligible (~0.2-3%) compared to instantaneous aerosol radiative forcing.

Regarding the aerosol shape, the AERONET solar flux estimates account for particle non-sphericity, a critical issue especially for mineral dust aerosols. Calculation of broadband radiative flux often does not consider particle non-sphericity. It is because the possible angular and spectral differences are expected to be canceled once all contributions of scattered light summed up into the total energy flux. Mishchenko et al. (1997) found that the Mie theory can be used for aerosol radiative effect calculations with adequate accuracy even for nonspherical aerosol particles. It was noted that using asymmetry parameter, which is an integrated value, the contrasting nonspherical-spherical differences in the aerosol phase function are averaged out during the integration. However, in AERONET flux estimates computations are conducted using not a limited integrated value of asymmetry parameter, but using twelve moments of phase function expansion that account for the details of the aerosol phase function. In addition, recalculating phase function at each step of spectral integration includes the spectral variations of the phase function. Using this type of computations, in a study by Derimian et al. (2008) it was shown that neglecting particle non-sphericity in the simulations of broadband fluxes in the presence of mineral dust results in an overestimation of aersosol radiative forcing by up to 10%.

In many studies in the literature, the aerosol radiative forcing simulations are carried out assuming no errors in the solar fluxes without aerosols or they are negligible with regard to the uncertainty of the observed measurements. Nonetheless, as found for the Mauna Loa Observatory, which is quite representative of a clear atmosphere, we have documented that its uncertainties are in the same range that those found under higher aerosol load. Hence, it is necessary to give special attention to this assumption because it seems to be not completely valid.

3. AERONET radiative forcing of key aerosol types

3.1 Description of key aerosol types

Atmospheric aerosols have a high temporal and spatial variability due to their different residence times in the atmosphere and the geographical distribution of their emission sources. This heterogeneity leads atmospheric aerosols to have differentiated size distributions and chemical compositions and, thus, different impacts on the radiative balance of the Earth-atmosphere system. These properties directly determine how atmospheric aerosols interact with the solar radiation and the relative importance between scattering and absorption processes. In order to account for this heterogeneity of aerosol radiative properties, this study examines the radiative effect of the individual aerosol species, emitted into the atmosphere from different source areas. Thus, the key aerosol types considered here have been shown to have an important influence on the radiative balance, according to their rates of emission into the atmosphere and to their radiative properties (Dubovik et al., 2002b; IPCC, 2007): desert mineral dust introduced into the atmosphere by erosive processes; biomass burning produced by farming activities and forest fires; urban-industrial, continental background, oceanic aerosols and those that are found in free troposphere conditions. Fig. 3 shows the scanning electron microscopy (SEM) observations of some of these atmospheric aerosols observed during MINATROC (MINeral dust Aerosol and TROpospheric Chemistry) campaign in 2002 in Tenerife (Canary Islands) (Alastuey et al., 2005): (a) spongy carbonaceous particles from urban-industrial combustion; (b) sodium chloride crystals from marine aerosols; (c) aggregates of micro-crystals of clay minerals

typical of mineral dust environments and (d) silica skeletons of fresh water diatom present in lakes or ponds from Northern Africa.

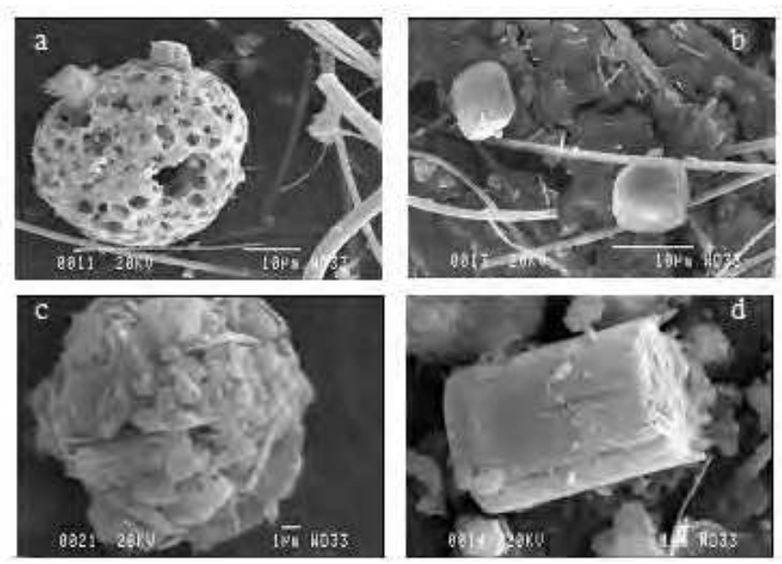

Fig. 3. SEM photographs of particle matter observed over Tenerife (Canary Islands) during the MINATROC campaign in 2002.

Following García et al. (2011b), in order to analyze the radiative effect of the aforementioned atmospheric aerosols a set of forty AERONET stations were selected (Fig. 4), which have been grouped into 14 regions to account for key aerosol types from different aerosol sources.

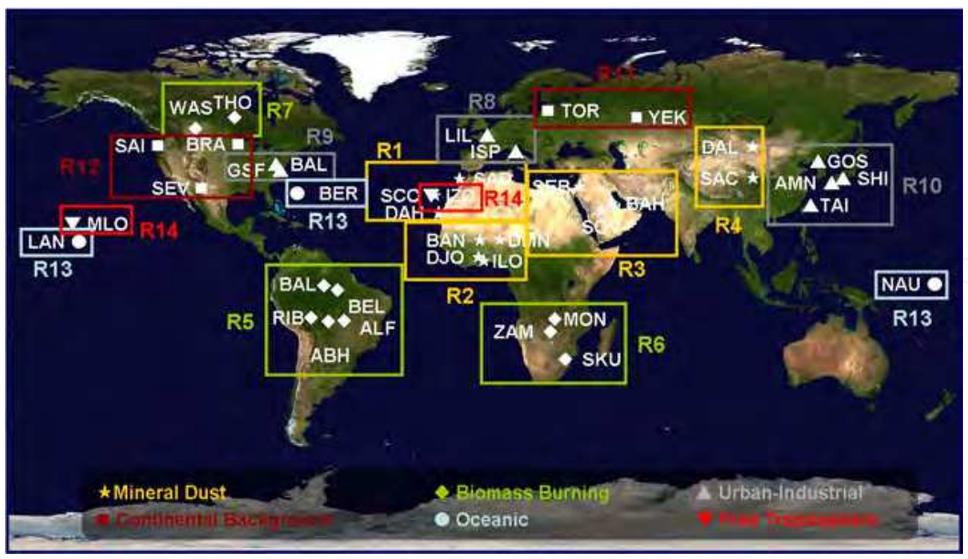

Fig. 4. Geographical distribution of the AERONET stations used. These stations were grouped into 14 regions (from R1 to R14), according to the key aerosol types and their geographic location (García et al., 2011b). Each aerosol type is labelled with a different color: mineral dust as yellow, biomass burning as green, urban-industrial as gray, background continental as brown, oceanic as blue and free troposphere as red.

3.1.1 Desert mineral dust

Desert mineral dust is one of the main aerosols emitted into the atmosphere on a global scale, and it therefore plays a decisive role in the radiative balance of the climatic system. In general, mineral dust particles show a high capacity for attenuating solar radiation (high AOD) and are mainly made up of large particles, which normally form aggregates of micro-crystals. The chemical and mineralogical composition of these particles strongly depends on the characteristics and composition of soils that generate them. For these reasons, this discussion is dedicated to mineral dust from the main desert dust areas of the world: the Sahara-Sahel desert area (distinguishing two regions: North, R1, and Central Africa, R2), the Middle East (Arabian Peninsula, R3) and the Taklamakan and the Gobi deserts (China and Mongolia, R4). All of these mineral dust regions are located within "dust belt" (5ºN-40ºN), where the mineral dust concentrations are maximal on a global scale (Prospero et al., 2002). Please refer to García et al. (2011b) for a detailed description of the AERONET stations used and the regions.

The mineral dust properties are clearly observed in the annual cycle of the inter-annual and regional average of the aerosol optical depth (AOD) and the single scattering albedo (ω) at 0.55 μm and the effective radius of the aerosol size distribution for all regions (Fig. 5, Fig. 6 and Fig. 7 respectively). The ω is a measure of the effectiveness of scattering relative to total extinction for the light encountering the atmospheric aerosol particles (the ratio of scattering optical depth to the total optical depth), while the effective radius is an area weighted mean radius of the aerosol particles. The combination of AOD, ω and effective radius information allows us to describe and discriminate aerosols with similar solar extinction but different sizes, such as mineral dust and biomass burning particles. An example is the contribution of biomass burning particles due to farming activities during the dry season (winter) in the Central Africa region (R2). In this season high AOD values are associated with a clear decrease of the ω and the effective radius in contrast to spring, where the mineral dust is the predominant aerosol and, thus, larger particles with a lower absorption at 0.55 μm are observed.

In order to guarantee the quality of the AERONET ω estimations this magnitude is only retrieved for high aerosol load (AOD (0.44 μm)≥0.4) (Dubovik et al., 2002b; 2000).

3.1.2 Smoke from vegetation fires

Biomass burning aerosols are dominated by fine particles of black carbon and organic material from forest fires of local and regional farming activities, mainly from the tropical regions of Amazonian forest (R5) and African savannah (R6) (25ºS-25ºN) during the dry season. Their radiative properties are mainly given by the different material composition and combustion processes associated with their production (with or without flames). Thus, in the African savannah, most biomass burning particles are produced by means of flaming combustion, while in deforestation fires, typical of Amazon forest, ~50% or less of the biomass burning is produced by this phase of combustion. These different production mechanisms lead to different concentrations of black carbon: 15-20% of the aerosols generated during the flaming combustion phase correspond to black carbon while less than 3% are generated during smouldering combustion (García et al., 2011b and references therein) and, thus, significant differences occur for the single scattering albedo (Fig. 6.b).

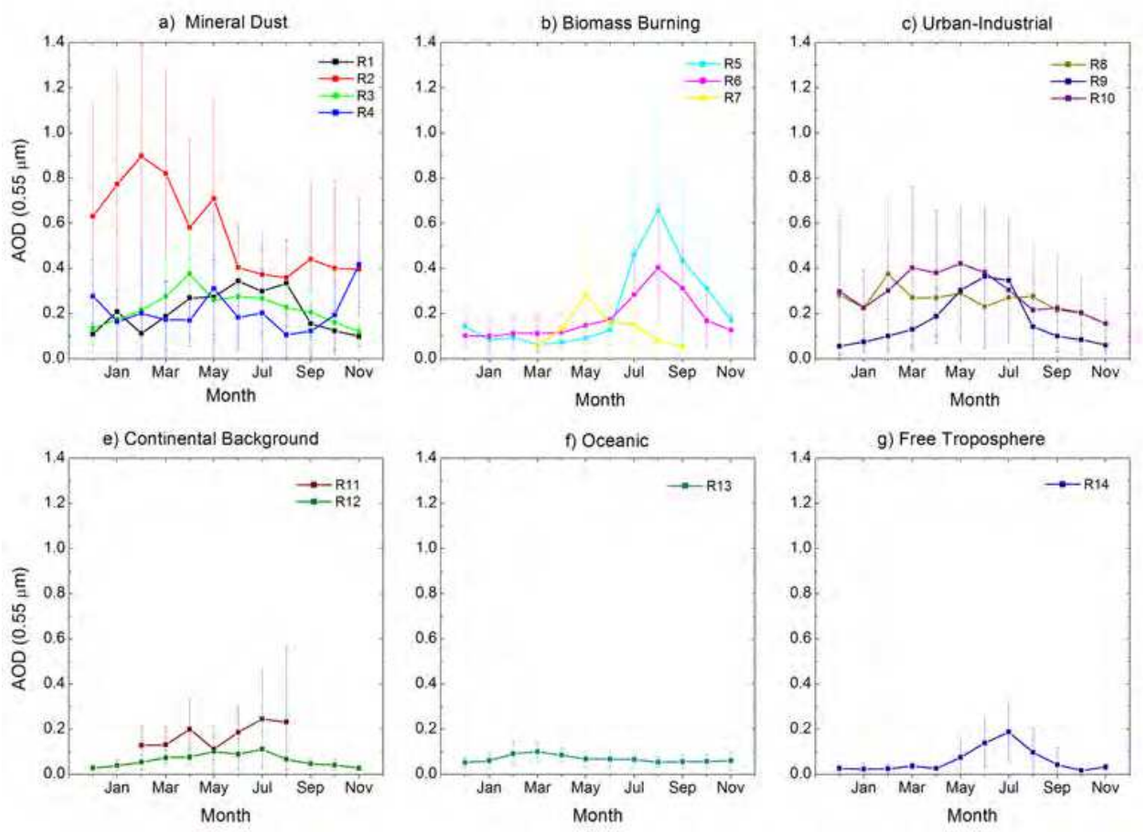

Fig. 5. Annual cycle of the inter-annual average of the aerosol optical depth (AOD) at 0.55 µm for the key aerosol types grouped into 14 regions. Error bars indicate 1σ (standard deviation).

Together with the production of biomass burning due to agriculture, this aerosol is also produced, but to a lesser extent, in fortuitous or provoked forest fires over the continental platforms of North America and Eurasia (R7). These fires occur almost exclusively during summer, when meteorological conditions are more favourable. In these cases the smouldering combustion aerosols are majority (Dubovik et al., 2002b).

Besides the aerosol size, a clear difference between mineral dust and other aerosols, such as biomass burning or urban-industrial ones aerosols is the spectral dependence of the absorption properties. Mineral dust show the highest absorption at wavelengths close to the ultraviolet solar range in contrast to biomass burning and urban-industrial aerosols, where the absorption increases in the near infrared region (Dubovik et al., 2002b, Hess et al., 1998). Also, it should be noted that, while mineral dust was previously considered as strongly absorbing (e.g. Hess et al., 1998), Kaufman et al. (2001) and (Dubovik et al., 2002b) demonstrated using AERONET and satellite observations that mineral dust is practically does not absorb in visible and near infrared.

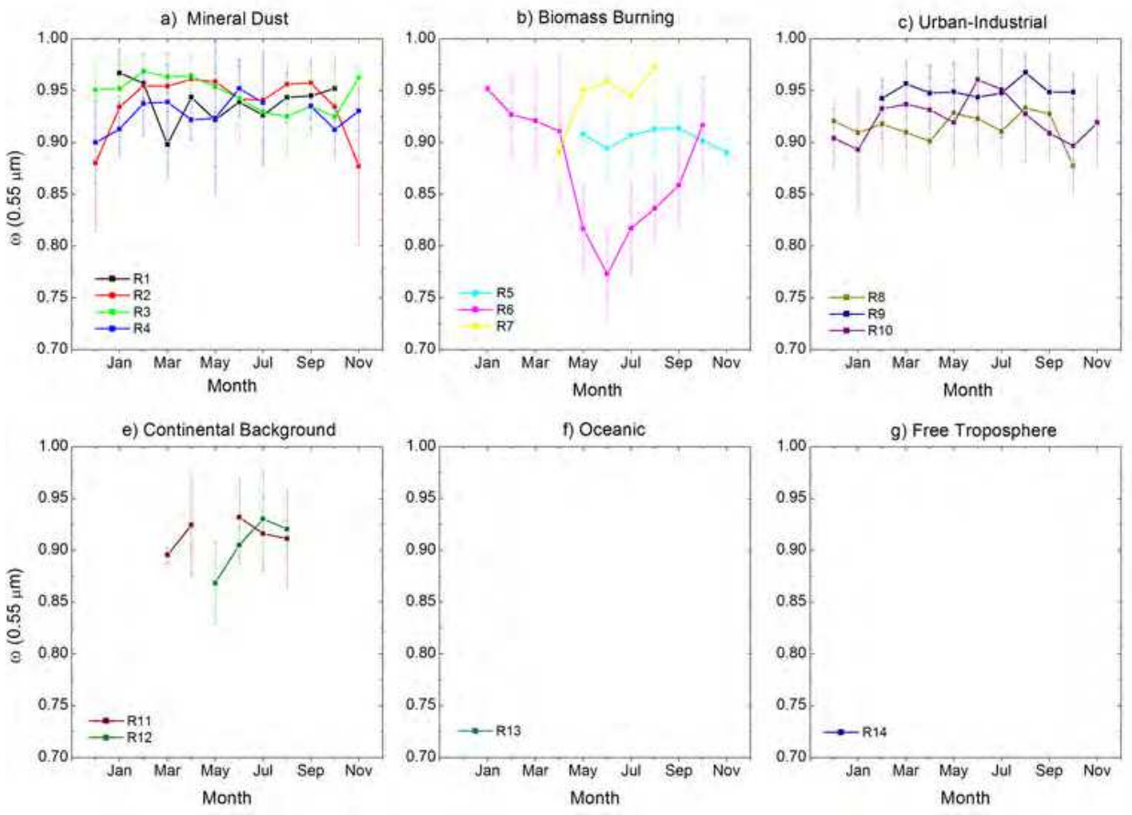

Fig. 6. Annual cycle of the inter-annual average of the aerosol single scattering albedo (ω) at 0.55 μm for the key aerosol types grouped into 14 regions. Error bars indicate 1σ (standard deviation).

3.1.3 Urban and industrial pollution

Urban-industrial aerosols are very small particles so the fine mode is predominant in the size distribution. The main sources of these aerosols are found in the most heavily populated and industrialized areas of the world, such as Europe (R8), the East and West coast of North America (R9) and Southeast Asia (R10). The industrial combustion processes, the population or even the regional meteorological conditions are responsible for the differences in their radiative properties. For example, although road traffic is a common source in all regions, and in some cases the main source of contamination, Europe has a higher proportion of diesel automobiles than United States (Dubovik et al., 2002b). Also, new chemical measurements show that downwind of the eastern United States the contribution of carbonaceous material to AOD (30%) is double that of sulphates (16%),with water intake (48%) and black carbon (6%) accounting for the rest (Kaufman & Koren, 2006). Hence, the American region exhibits a lower absorption capacity (see Fig. 6.c).

Note that in the Asiatic region there are notable episodes of mineral dust transport from the Gobi-Taklamakan deserts during spring and at the beginning of summer, which are responsible for the spring peak observed in the AOD and the effective radius annual cycles (Fig. 5.c and Fig. 7.c respectively).

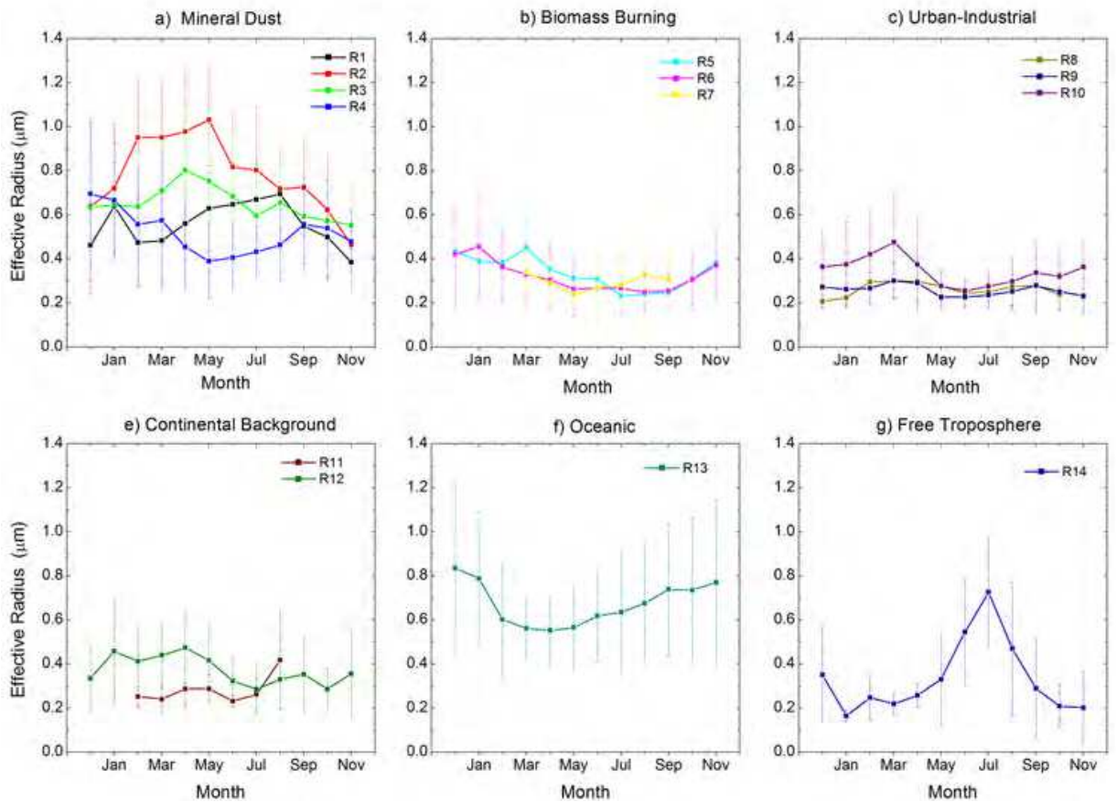

Fig. 7. Annual cycle of the inter-annual average of the effective radius (μm) for the key aerosol types grouped into 14 regions. Error bars indicate 1σ (standard deviation).

3.1.4 Background continental

Background continental aerosols are typical from non-industrial areas located over eastern European (R11) and American (R12) prairies, where the main aerosol type generally derives from continental sources, such as biogenic emissions from forests, re-suspension of particulate matter from grass and soil, etc. Normally, the presence of local anthropogenic pollution sources is not significant in these regions, although they may be affected by regional transport from nearby urban-industrial areas or forest fires. Therefore, they may show similar properties to urban-industrial (R8 and R9) and biomass burning aerosols from boreal forest fires (R7): exhibiting small sizes and a significant absorption (Fig. 7.d and Fig. 6.d respectively).

3.1.5 Oceanic aerosol

Sea spray generated from the surface of the seas and oceans is the most common component globally (R13). Nonetheless, they have a minor role in the solar radiative balance of the Earth-atmosphere system due to their low capacity for extinguishing solar radiation (low and stable AOD, Fig. 5.e). These particles are also characterized by a pronounced mode of coarse particles with effective radius of the order of mineral dust, except that oceanic aerosols have a spherical shape because of their hygroscopic character. These particles are normally the result of two physical processes: stirring the sea surface by wind and the rupture of air bubbles during the formation of sea foam.

3.1.6 Free troposphere

The atmospheric conditions for monitoring atmospheric aerosols in the free troposphere are very special. These measurements should be representative of natural background conditions. This difficult requirement is only met in a few high mountain observatories, which are exposed to a natural undisturbed atmosphere with minimal influences from natural ecosystem or human activities.

In order to evaluate the aerosol properties of the free troposphere (R14) two GAW (Global Atmospheric Watch) stations were considered: Mauna Loa and Izaña Observatories. Both places are located at a high altitude (2,367 and 3,397 m a.s.l. respectively) and above a thermal inversion layer, thus avoiding the contributions of natural and anthropogenic aerosols. The exceptions are episodes of African desert mineral dust measured at the Izaña station during the summer, months of greatest activity in the North Sahara-Sahel region. Thus, these events are responsible for the marked increase of AOD and effective radius observed in the free troposphere region during summer (Fig. 5.f and Fig. 7.f respectively).

In order to estimate a budget of aerosol emissions, the frequency of occurrence of those situations with a high extinction of solar radiation has been computed for each region and aerosol type (Fig. 8). For that, we have only considered cases with AOD (0.44 μm)≥0.4 according to AERONET's high quality threshold. The Central Africa region (R2) clearly shows the highest number of cases that exceeds the AOD limit, 32% of those analyzed, in contrast to 15% in the Arabian mineral dust or values lower than 5% in the other regions under mineral dust. Regarding biomass burning regions, the African savannah has the majority impact on the AOD levels (~15%) and doubles the cases observed in the Amazonian region. This latter region and the urban-industrial areas show similar percentages, ~8%, while for background continental regions they represent less than 1% of the total. Finally, in the oceanic and the free troposphere regions there are no situations that fulfilled the AOD threshold.

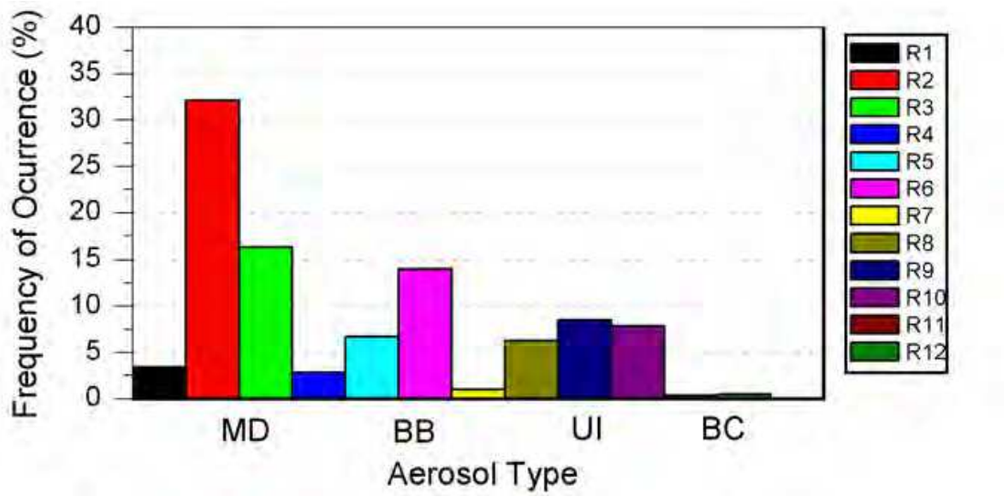

Fig. 8. Frequency of Occurrence (%) of cases with AOD (0.44 μm)≥0.4 for the key aerosol types grouped into 14 regions. The key aerosol types are labelled as: MD≡Mineral Dust; BB≡Biomass Burning; UI≡Urban-Industrial; BC≡Background Continental; O≡Oceanic and FT≡Free Troposphere.

3.2 Radiative Forcing at the BOA and at the TOA

As aforementioned, AERONET computes the direct radiative forcing at the BOA and at the TOA in order to study the effect of atmospheric aerosols on the climate system. The high density of the AERONET stations allows for a detailed analysis of ΔF and thus the estimates of the total radiative effect of key aerosol types.

The aerosol radiative forcing strongly depends on the total aerosol extinction (AOD), the solar geometry and the surface type. This latter parameter is especially critical in estimating the ΔF at the TOA, since a clear decrease of the ΔF absolute values has been documented as surface reflectivity increases, even changing the sign of the radiative forcing. Recent studies found that over dark surfaces (oceanic and vegetative covers, i.e., surface reflectivity, SR, lower than 30%) atmospheric aerosols always cool the Earth-atmosphere system, regardless of aerosol type (García et al., 2011a, 2011b). Nonetheless, over the brightest surfaces, the total radiative effect depends on the aerosol absorption properties and on the SR values. Therefore, in order to make a consistent comparison of the net aerosol effect, the analysis has been partitioned into two ranges of surface reflectivity: SR≤30% and SR>30%. Besides, the data shown are limited at sza of 60±5º to take the nearly same geometry into account.

The annual evolution of the ΔF is mainly determined by the annual variations of total aerosol extinction (AOD), as shown in Fig. 9 and 10 (ΔF values at the BOA, eq. 1, and at the TOA, eq. 2, respectively for SR≤30%). Thus, the ΔF annual cycle of each key aerosol type, both at the BOA and the TOA, perfectly follows its respective AOD annual evolution (see Fig. 5). The highest annual ΔF amplitude (in absolute value) is observed for the mineral dust regions, while the oceanic aerosols present the flattest ΔF annual cycle. The lowest ΔF is observed for the free tropospheric region, however its amplitude variations present a significant peak value in summer, associated with the arrival of mineral dust from the Saharan desert to the Izaña station. The biomass burning aerosols also show a clear seasonality, increasing the ΔF values (in absolute value) during the biomass burning season (from July to December). Finally, the urban-industrial regions have a wide ΔF amplitude mainly from January to August. It is important to mention that the ΔF inter-annual averages were negative for all regions both at the BOA and the TOA, denoting a global cooling effect by atmospheric aerosols.

The maximal values of ΔF at the BOA and at the TOA are found in the Central Africa region during winter, associated with the mixture of mineral dust from the Sahara-Sahel desert and biomass burning aerosols, around -180 Wm^{-2} at the BOA and higher than -40 Wm^{-2} at the TOA. During the summer period (wet season) the ΔF values are comparable to other mineral dust regions or other aerosol species (like biomass burning or urban-industrial particles). In this region, we also found the highest AOD levels among those analyzed. Furthermore, it is remarkable the peak observed in the biomass burning regions from South America and South Africa during the fall, a period of maximal biomass burning activity, with ΔF values higher than -80 Wm^{-2} at the BOA and around -40 Wm^{-2} at the TOA. These values are even more important than Saharan (R1), Arabian (R3) and Asian (R4) mineral dust and of the order of those observed under urban-industrial environments. These latter regions correspond to the most industrialized areas in the world (Southeast Asia, Europe and the East coast of North America), where their radiative forcing values range between 0 and -80 Wm^{-2} at the BOA and from 0 to -40 Wm^{-2} at the

TOA, during the first half of the year, diminishing slightly in the second half. Regarding the areas dominated by background continental aerosols, the results show that the forcing values in the European region (R11) are double those observed in the American region (R12). Finally, the lowest values of forcing are obtained in the oceanic region and under free troposphere conditions, with values lower than -10 Wm^{-2} both at the BOA and at the TOA.

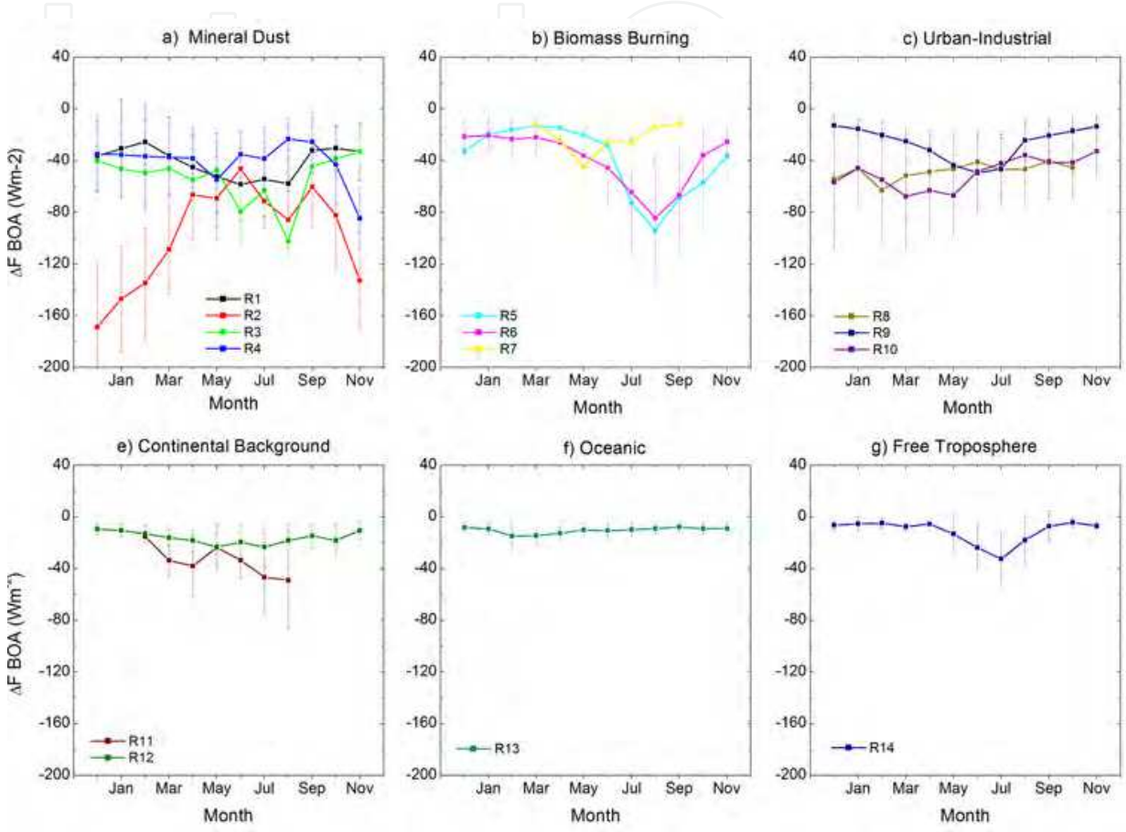

Fig. 9. Annual cycle of the inter-annual average of the aerosol radiative forcing (ΔF, Wm^{-2}) at the BOA for the key aerosol types grouped into 14 regions and for surface reflectivity SR≤30%. Error bars indicate 1σ (standard deviation)

The BOA radiative forcing provides decrease of the solar radiation at the surface due to scattering of radiation back to space and due to trapping of radiation in the atmospheric layer. Therefore, decrease of the solar radiation at the surface in conjunction with low aerosol scattering effectiveness (low single scattering albedo) indicates increase of radiation trapped in the atmospheric layer due to aerosol absorption, which is directly related to the aerosol semi-direct effect. This absorption produces an atmospheric temperature gradient contributing to the modification of atmospheric dynamic and cloud characteristics. As can be seen from Fig. 9 the most significant BOA forcing occurs in the Amazonian, South Africa and Central Africa regions. The Amazonian and South Africa are known as biomass burning regions, while the Central Africa in winter time is characterised by the mixture of mineral dust and biomass burnings particles, in all these cases the single scattering albedo (Fig. 6) is low presenting important aerosol absorption.

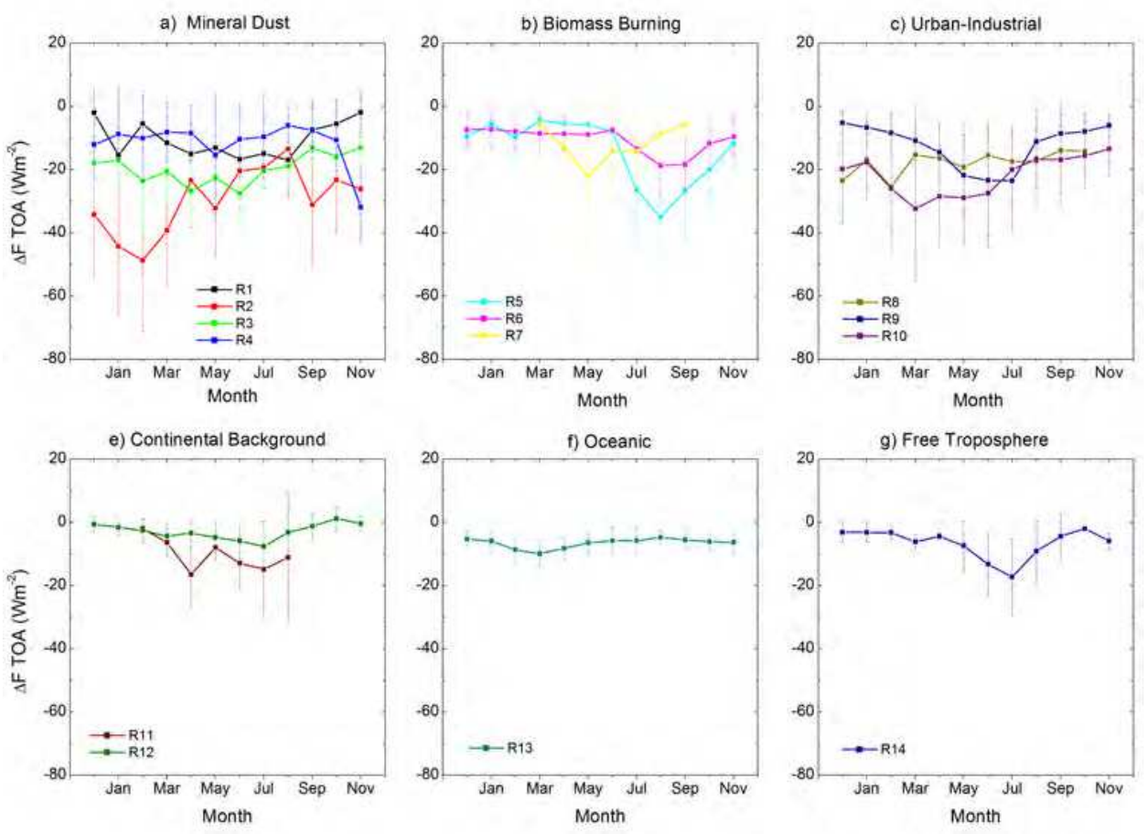

Fig. 10. Annual cycle of the inter-annual average of the aerosol radiative forcing (ΔF, Wm^{-2}) at the TOA for the key aerosol types grouped into 14 regions and for surface reflectivity SR≤30%. Error bars indicate 1σ (standard deviation).

How atmospheric aerosols affect cloud cover (increase or decrease) is one of the largest uncertainties in climate models (IPCC, 2007). In fact, recent studies show that heavy smoke over the Amazon forest and pollution over China decrease the cloud cover by heating the atmosphere and cooling the surface and these effects may balance some of the large negative aerosol forcing (Kaufman & Koren, 2006, and references therein). Likewise, Satheesh & Ramanathan (2000) have shown that, over the tropical Indian Ocean during winter months, absorbing aerosols produce important atmospheric heating, which is translated into a diurnal mean heating rate perturbation. Therefore, the assessment of the seasonal variations in the ΔF values at the BOA and at the TOA presented here is fundamental to document properly these aerosol effects in climate modelling both at the regional and global scale. Furthermore, the cloud properties, one of the most crucial climatic elements, strongly depend on these seasonal behaviours.

On the other hand, a very interesting issue is to observe whether there are differences in radiative forcing when the different aerosol types under study are grouped according to their origin. Thus, the regions R1, R2, R3, R4, R7, R13 and R14 were considered as natural, and the regions R5, R6, R8, R9 and R10 as anthropogenic. With this selection we

determine that the natural aerosols carry the most weight in the radiative balance. The ΔF annual average at BOA for anthropogenic aerosols is -88±36 Wm^{-2} (AOD=0.54±0.28 at 0.55 μm) while it is -121±47 Wm^{-2} (AOD=0.77±0.43) for natural aerosols. The ΔF at the TOA for anthropogenic aerosols is -31±15 Wm^{-2} versus -36±20 Wm^{-2} observed for natural aerosols.

The influence of the surface reflectivity on ΔF is clearly observed, for example, for the mineral dust regions (Fig. 11), especially at the TOA. Thus, reductions of the absolute values of the ΔF are documented for surfaces with SR higher than 30%, reaching even positive mean values. In these latter cases, atmospheric aerosols lead to a warming of the Earth-atmosphere system, contributing to the GHGs effect.

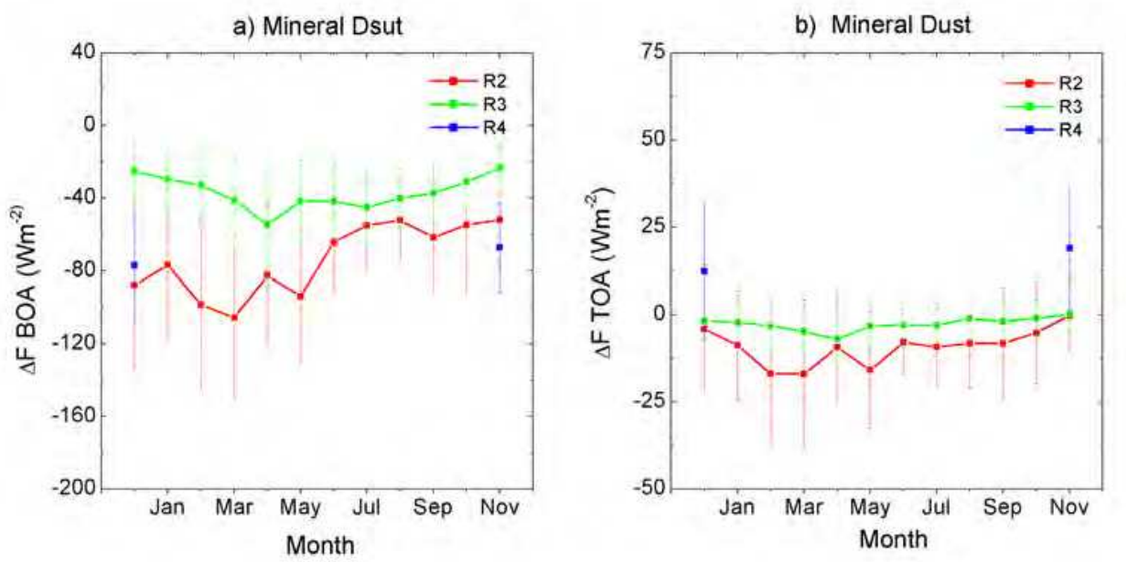

Fig. 11. Annual cycle of the inter-annual average of the aerosol radiative forcing (ΔF, Wm^{-2}) at the BOA (a) and at the TOA (b) for surface reflectivity SR>30% for the mineral dust regions. Error bars indicate 1σ (standard deviation).

From a global perspective, table 1 summarizes the annual and regional radiative forcing averages at the BOA, TOA and the AOD at 0.55 μm, considering together the whole range of surface reflectivity. Note that in order to compute mean values representative of the free troposphere on a global scale the period with possible mineral dust events at the Izaña Observatory were ruled out here. The results allow us to quantify, in clear sky conditions, the relative influence of each key aerosol type as well as the importance of the different mechanisms for modifying the energy balance of the Earth-atmosphere system (directly or by storing energy in the system). These mean values may be considered as a first reference at solar zenith angles of 60±5º, although it would be necessary to estimate annual average values from the daily radiative forcing values in order to make more solid conclusions.

Aerosol Type	Region	ΔF_{BOA} (Wm^{-2})	ΔF_{TOA} (Wm^{-2})	AOD (0.55 μm)
MD	R1	-44±28	-11±12	0.23±0.20
MD	R2	-89±51	-16±22	0.58±0.46
MD	R3	-40±23	-4±9	0.23±0.17
MD	R4	-41±32	-8±15	0.20±0.20
BB	R5	-54±45	-19±18	0.33±0.37
BB	R6	-46±37	-11±8	0.21±0.18
BB	R7	-24±26	-13±15	0.14±0.20
UI	R8	-48±30	-18±15	0.27±0.24
UI	R9	-25±20	-11±11	0.15±0.17
UI	R10	-49±34	-20±15	0.28±0.24
BC	R11	-37±22	-7±14	0.17±0.16
BC	R12	-17±12	-3±6	0.17±0.16
O	R13	-10±6	-7±4	0.07±0.04
FT	R14	-6±3	-5±3	0.03±0.01

Table 1. Annual and regional average and standard deviation of ΔF_{BOA} (Wm^{-2}), ΔF_{TOA} (Wm^{-2}) and AOD at 0.55 μm for the key aerosol types grouped into 14 regions. The key aerosol types are labelled as: MD≡Mineral Dust; BB≡Biomass Burning; UI≡Urban-Industrial; BC≡Background Continental; O≡Oceanic and FT≡Free Troposphere.

4. Conclusions

Atmospheric aerosols play an essential role in the configuration of the radiative balance of the Earth-atmosphere system. The spatial and temporal heterogeneity of their physical-chemical properties makes global networks fundamental tools for their complete characterization. Likewise, atmospheric aerosols are a decisive factor for modifying cloud properties, since they serve as cloud condensation nuclei, and hence affect the hydrological cycle as well. Moreover, those species with important absorption properties may lead to an unequal warming of the atmosphere and may also modify cloud formation and cloud cover. Therefore, improving our knowledge about the direct radiative effects of atmospheric aerosols is a necessary step in order to address the indirect and semi-direct aerosol effects.

In this context, AERONET is today the most important network for monitoring atmospheric aerosols. AERONET aerosol products are widely used by the international research community to compute aerosol climatologies, to provide data for climate models and to validate space-based sensors. Thus, this chapter presents valuable information, describing and summarizing an approach for estimating broadband solar fluxes and hence the direct radiative forcing of atmospheric aerosols from AERONET retrievals. A detailed description of the radiative transfer model and its inputs has been shown as well as the uncertainties to be expected by comparing with observations of insolation. Finally, the direct radiative forcing of key aerosol types has been analyzed: mineral dust, biomass burning, urban-industrial, background continental, oceanic and in free troposphere. These magnitudes have been evaluated at the surface and at the top of the atmosphere, allowing us to document the actual and net radiative balance of these aerosol types.

A next important step for this work would be to exploit the cloud products recently released by AERONET in order to make a more complete description of the relationships between aerosols, clouds and the energy budget in the Earth-atmosphere system. These new products, together with the information obtained from space-based and ground-based sensors, mainly the A-Train satellite constellation, will promote a deeper knowledge of the processes affecting cloud properties.

5. Acknowledgements

We acknowledge to the MEC (Ministry of Education and Science, Spain) for the following support: projects CGL2008-04740/CLI and CGL2010-21366-C04-01. We gratefully acknowledge the data provided by the AERONET network and we wish to express our appreciation to the operators of the stations for their help in operating the instruments.

6. References

Ackerman, A. S., Toon, O. B., Stevens, D. E., Heymsfield, A. J., Ramanathan, V. &Welton, E. J. (2000). *Reduction of tropical cloudiness by soot*, Science 288: 1,042–1,047.

Alastuey, A., Querol, X., Castillo, S., Escudero, M., Ávila, A., Cuevas, E., Torres, C., Romero, P. M., Expósito, F. J., García, O. E., Díaz, J. P., Dingenen, R. V. & Putaud, J. P. (2005). *Characterisation of TSP and PM2.5 at Izaña and Santa Cruz de Tenerife (Canary Island, Spain) during a Saharan dust episode (July 2002)*, Atmos. Environ. 39: 4,715–4,728.

Charlson, R. J., Lovelock, J. E., Andreae, M. O. &Warren, S. G. (1987). *Oceanic phytoplankton, atmospheric sulphur, cloud albedo and climate*, Nature 326: 655–661.

Derimian, Y., León, J.-F., Dubovik, O., Chiapello, I., Tanré, D., Sinyuk, A., Auriol, F., Podvin, T., Brogniez, G. & Holben, B. N. (2008). *Radiative properties of aerosol mixture observed during the dry season 2006 over m0bour, Senegal (African monsoon multidisciplinary analysis campaign)*, J. Geophys. Res. 113.

Dubovik, O. & King, M. D. (2000). *A flexible inversion algorithm for retrieval of aerosol optical properties from sun and sky radiance measurements*, J. Geophys. Res. 105: 20,673–20,696.

Dubovik, O., Smirnov, A., Holben, B. N., King, M. D., Kaufman, Y. J., Eck, T. F. & Slutsker, I. (2000). *Accuracy assessment of aerosol optical properties retrieval from AERONET sun and sky radiance measurements*, J. Geophys. Res. 105: 9791–9806.

Dubovik, O., Holben, B. N., Lapyonok, T., Sinyuk, A., Mishenko, M. I. & Slustker, I. (2002a). *Non-spherical aerosol retrieval method employing light scattering by spheroids*, Geophys. Res. Lett. 29: 54–1 – 54–4.

Dubovik, O., Holben, B. N., Eck, T. F., Smirnov, A., Kaufman, Y. J., King, M. D., Tanré, D. & Sluster, I. (2002b). *Variability of absorption and optical properties of key aerosol types observed in worlwide locations*, J. Atmos. Sci. 59: 590–608.

Dubovik, O., Sinyuk, A., Lapyonok, T., Holben, B. N., Mishchenko, M., Yang, P., Eck, T. F., Volten, H., Munoz, O., Veihelmann, B., van der Zande, W. J., Leon, J.-F., Sorokin, M. & Slutsker, I. (2006). *Application of light scattering by spheroids for accounting for particle non-sphericity in remote sensing of desert dust*, J. Geophys. Res. 111.

Dubovik, O., Herman, M., Holdak, A., Lapyonok, T., Tanré, D., Deuzé, J. L., Ducos, F., Sinyuk, A. & Lopatin, A. (2011*). Statistically optimized inversion algorithm for enhanced retrieval of aerosol properties from spectral multi-angle polarimetric satellite observations*, Atmos. Meas. Tech. 4: 975–1,018.

Dubuisson, P., Buriez, J. C. & Fouquart, Y. (1996). *High spectral resolution solar radiative transfer in absorbing and scattering media, Appliation to the sattelite simulations*, J. Quant. Spectrosc. Radiat. Transfer 55: 103–126.

Dubuisson, P., Dessailly, D., Vesperini, M. & Frouin, R. (2004). *Water vapor retrieval over ocean using near-infrared imagery*, J. Geophys. Res. 109.

Dutton, E. G., Michalsky, J. J., Stoffel, T., Forgan, B.W., Hickey, J., Nelson, D.W., Alberta, T. L. & Reda, I. (2001*). Measurements of broadband diffuse solar irradiance using current commercial instrumentation with a correction of thermal offset errors*, J. Atmos. Oceanic Technol. 18: 297–314.

Eck, T. F., Holben, B. N., Reid, J. S., Dubovik, O., Smirnov, A., ON´ eill, N. T., Slustker, I. & Kinne, S. (1999). *Wavelength dependence of the optical depth of biomass burning, urban, and desert dust aerosols*, J. Geophys. Res. 104.

García, O. E., Díaz, A. M., Expósito, F. J., Díaz, J. P., Dubovik, O., Dubuisson, P., Roger, J.-C., Eck, T. F., Sinyuk, A., Derimian, Y., Dutton, E. G., Schafer, J. S., Holben, B. & García, C. A. (2008). *Validation of AERONET estimates of atmospheric solar fluxes and aerosol radiative forcing by ground-based broadband measurements*, J. Geophys. Res. 113.

García, O. E., Expósito, F. J., Díaz, J. P. & Díaz, A. M. (2011a). *Radiative forcing under aerosol mixed conditions*, J. Geophys. Res. 116.

García, O. E., Expósito, F. J., Díaz, J. P., Díaz, A. M., Dubovik, O., Derimian, Y., Dubuisson, P. & Roger, J.-C. (2011b). *Shortwave radiative forcing and efficiency of key aerosol types using AERONET data*, Atmos. Chem. Phys. Discuss. 11, 1–38, 2011

Hansen, J., Sato, M., Kharecha, P. & von Schuckmann, K. (2011). *Earth's energy imbalance and implications*, Atmos. Chem. Phys. Discuss. 11: 27,031–27,105.

Haywood, J., Francis, P., Osborne, S., Glew, M., Loeb, N., Highwood, E., Tanré, D., Myhre, G., Formenti, P. & Hirst, E. (2003). *Radiative properties and direct radiative effect of saharan dust measured by the c-130 aircraft during shade: 1. solar spectrum*, J. Geophys. Res. 108.

Hess, M., Koepke, P. & Schult, I. (1998). *Optical properties of aerosols and clouds: the software pagckage OPAC*, Bull. Am. Meteor. Soc. 79: 831–844.

Holben, B. N., Eck, T. F., Slutsker, I., Tanré, D., Buis, J. P., Setzer, A., Vermote, E., Reagan, J. A., Kaufman, Y., Nakajima, T., Lavenu, F., Jankowiak, I. & Smirnov, A. (1998). *AERONET - a federated instrument network and data archive for aerosol characterization*, Remote Sens. Environ. 66: 1–16.

IPCC (2007). *The Physical Science Basis, Fourth Assessment Report Summary*, Intergovernmental Panel on Climate Change, Cambridge University Press, New York.

Kaufman, J. Y., Tanré, D., Dubovik, O., Karnieli, A. & Remer, L.A. (2001) *Absorption of sunlight by dust as inferred from satellite and ground-based remote* sensing, Geophys. Res. Lett. 28:1,479-1,483.

Kaufman, Y. & Koren, I. (2006). *Smoke and pollution aerosol effect on cloud cover*, Science 313.

Koren, I., Kaufman, Y.J., Remer, L.A. & Martins, J.V.(2004). *Measurement of the effect of Amazon smoke on inhibition of cloud formation*, Science *303*:1,342-1,345.

Lohmann, U. & Feichter, J. (2005*). Global indirect aersools effects: a review*, Atmos. Chem. Pys. 5: 715–737.

Michalsky, J., Dutton, E., Rubes, M., Nelson, D., Stoffel, T., Wesley, M., Splitt, M. & DeLuisi, J. (1999). *Optimal measurements of surface shortwave irradiance using current instrumentation*, J. Atmos. Oceanic Technol. 16: 55–69.

Mishchenko, M. I., Travis, L. D., Kahn, R. A. & West, R. A. (1997). *Modeling phase functions for dustlike tropospheric aerosols using a shape mixture of randomly oriented polydisperse spheroids*, J. Geophys. Res. 102: 16,831–16,847.

Myhre, G., Berntsen, T. K., Haywood, J. M., Sundet, J. K., Holben, B. N., Johnsrud, M. & Stordal, F. (2003). *Modeling the solar radiative impact of aerosols from biomass burning during the southern african reginal science iniative (safari-2000) experiment*, J. Geophys. Res. 108.

Nakajima, T. & Tanaka, M. (1988). *Algorithms for radiative intensity calculations in moderately thick atmospheres using a truncation approximation*, J. Quant. Spectrosc. Radiat. Transfer 40: 51–69.

Prospero, J. M., Ginoux, P., Torres, O., Nicholson, S. E. & Grill, T. E. (2002). *Environmental characterization of global sources of atmospheric soil dust identified with the NIMBUS 7 Total Ozone Mapping Spectrometer (TOMS) absorbing aerosol product*, Rev. Geophys. 40.

Roger, J.-C., Mallet, M., Dubuisson, P., Cachier, H., Vermote, E., Dubovik, O. & Despiau, S. (2006). *A synergetic approach for estimating the local direct aerosol forcing: Applications to an urban zone during the ESCOMPTE experiment*, J. Geophys. Res. 111.

Satheesh, S. K. & Ramanathan, V. (2000). *Large differences in tropical aerosol forcing at the top of the atmosphere and earth's surface,* Nature 405: 60–62.

Sinyuk, A., Dubovik, O., Holben, B., Eck, T. F., Breon, F.-M., Martonchik, J., Kahn, R., Diner, D. J., Vermote, E. F., Roger, J.-C., Lapyonok, T. & Slutsker, I. (2007*). Simultaneous retrieval of aerosol and surface properties from a combination of AERONET and satellite data*, Rem. Sens. Environ. 107: 90–108.

Smirnov, A., Holben, B.N., Eck, T.F., Dubovik, O. & Slutsker, I. (2000*) Cloud screening and quality control algorithms for the AERONET data bas*e, Rem. Sens. Environ. 73:337-349.

Stamnes, K., Tsay, S. C., Wiscombe, W. & Jayaweera, K. (1988). *Numerically stable algorithm for discrete-ordinate-method radiative transfer in multiple scattering and emitting layered media*, Appl. Opt. 27: 2,502–2,509.

Twomey, S. (1977). *Atmospheric aerosols*, New York, USA.

Zhou, M., Y., H., Dickinson, R., Dubovik, O. & Holben, B. N. (2005). *A normalized description of the direct effect of key aerosol types on solar radiation as estimated from Aerosol Robotic Network aerosols and Moderate Resolution Imaging Spectroradiometer albedos*, J. Geophys. Res. 110.

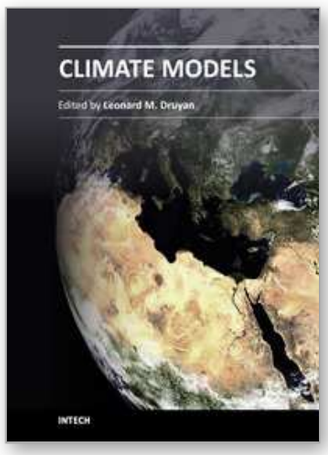

Climate Models

Edited by Dr. Leonard Druyan

ISBN 978-953-51-0135-2
Hard cover, 336 pages
Publisher InTech
Published online 02, March, 2012
Published in print edition March, 2012

Climate Models offers a sampling of cutting edge research contributed by an international roster of scientists. The studies strive to improve our understanding of the physical environment for life on this planet. Each of the 14 essays presents a description of recent advances in methodologies for computer-based simulation of environmental variability. Subjects range from planetary-scale phenomena to regional ecology, from impacts of air pollution to the factors influencing floods and heat waves. The discerning reader will be rewarded with new insights concerning modern techniques for the investigation of the natural world.

How to reference

In order to correctly reference this scholarly work, feel free to copy and paste the following:

O.E. García, J.P. Díaz, F.J. Expósito, A.M. Díaz, O. Dubovik and Y. Derimian (2012). Aerosol Radiative Forcing: AERONET-Based Estimates, Climate Models, Dr. Leonard Druyan (Ed.), ISBN: 978-953-51-0135-2, InTech, Available from: http://www.intechopen.com/books/climate-models/aerosol-radiative-forcing-aeronet-based-estimates

INTECH
open science | open minds

InTech Europe
University Campus STeP Ri
Slavka Krautzeka 83/A
51000 Rijeka, Croatia
Phone: +385 (51) 770 447
Fax: +385 (51) 686 166
www.intechopen.com

InTech China
Unit 405, Office Block, Hotel Equatorial Shanghai
No.65, Yan An Road (West), Shanghai, 200040, China
中国上海市延安西路65号上海国际贵都大饭店办公楼405单元
Phone: +86-21-62489820
Fax: +86-21-62489821

IntechOpen